Si-doped Al2o3 Nanosheet Supported Pd for Catalytic Combustion of Propane: Effects of Si Doping on Morphology, Thermal Stability and Water-resistance

Mingxiang Jiang
East China University of Science and Technology
Qingqing Wu
East China University of Science and Technology
Jiaorong Yan
East China University of Science and Technology
Jun Pan
Nanjing Engineering Institute of Aircraft Systems
Qiguang Dai
East China University of Science and Technology
Wangcheng Zhan (zhanwc@ecust.edu.cn)
East China University of Science and Technology

Research Article

Keywords: Catalytic combustion, Propane, Al2O3 nanosheet, Si doping, Thermal stability

Posted Date: April 16th, 2021

DOI: https://doi.org/10.21203/rs.3.rs-381545/v1

Abstract

Catalytic combustion of propane as typical light alkanes was important for the purification of industrial VOCs and automobile hydrocarbon emissions. Si-doped Al_2O_3 nanosheet was synthesized by a hydrothermal method, and effects of Si content on the morphology and thermal stability of Al_2O_3 were investigated. The doping of SiO_2 could tune the thickness of Al_2O_3 nanosheets and significantly improve its thermal stability, the θ phase was still maintained and the specific surface area was as high as 56.3 $m^2 \bullet g^{-1}$ after calcination at 1200 ℃. And then the Si-doped Al_2O_3 nanosheets were used as support of Pd catalysts (Pd/Si-Al_2O_3 nanosheets) for catalytic combustion of propane, especially Pd/3.6Si-Al_2O_3 nanosheets, which presented high activity, stability and resistance to sintering and H_2O due to the promotion of Si on the thermal stability of Al_2O_3 and the stabilization (dispersion, isolation and strong interaction) of PdO_x species.

1. Introduction

Volatile organic compounds (VOCs) were tightly controlled due to their toxicity and involvement in the formation of photochemical smog, and catalytic combustion was recognized the most efficient technique to eliminate VOCs emission (He et al 2019; Liu et al 2016; Han et al 2017). Light hydrocarbons (HCs) such as methane, ethane and propane were considered to be extremely difficult to be oxidized due to their high stability of molecular structures, which were produced from automotive exhaust or industrial processes, such as natural gas vehicle (NGV), liquefied petroleum gas (LPG) vehicles and stationary power source (Siegl et al 1999; Lai et al 2009; Lin et al 2020; Rahman 2019). Among HCs, propane was commonly selected as the model reaction to investigate the catalytic activity for unburnt HCs oxidation in gasoline vehicles exhaust and other VOCs in industrial processes. At present, different catalytic materials were employed to investigate the catalytic combustion of propane, Co_3O_4 and Ru based catalysts were identified as the most active materials for propane oxidation (Wang et al 2019; Hu et al 2018; Liu et al 2009). Liu found that nanocrystalline Co_3O_4 catalysts synthesized by a low-temperature liquid phase complexation method with different small molecular carboxylic acids presented a high activity (the conversion of propane reached 90% at 250°C) and stability (at least 40 h) (Liu et al 2009). Cai also confirmed that Co_3O_4/γ-Al_2O_3 was a high-active for propane combustion and developed a facile reduction-passivation approach to produce more abundant active cobalt oxides (Cai et al 2020). Hu reported the complete oxidation of propane on Ru/CeO_2 could be achieved below 200°C, due to the rich oxygen storage capacity of CeO_2 host, which can provide a large amount of active oxygen to RuO_x for propane oxidation (Hu et al 2018). However, the high temperature of vehicles exhaust even above 1050°C was a tremendous challenge for Co_3O_4 and Ru based catalysts, thus, the supported noble metals were still the most promising candidate due to their high thermal stability (Rahmati et al 2020; Yang et al 2019; Khairudin et al 2021).

However, the enhanced resistance to sintering of noble metals was still desired, and the highly stable support with the strong metal-support interaction (SMSI) such as stabilized γ-Al_2O_3 was one of the feasible strategies (Busca 2014). Generally, the bulk doping or surface modification such as SiO_2(Zheng et al 2016), TiO_2 (Chen et al 2019), CeO_2 (Cargnello et al 2012), La_2O_3 (Jing et al 2019; Zhou et al 2014), MgO (Zhan et al 2019) and NiO_2 (Fang et al 2015) was considered an effective strategy to improve high temperature stability of γ-Al_2O_3 to obtain the stabilized γ-Al_2O_3. Masakuni Ozawa studied the existence of a strong interaction between the La and Al_2O_3 by characterizing the surface, structural and chemical properties of La-doped γ-Al_2O_3 (Ozawa et al 2016). However, the introduction of La into the γ-Al_2O_3 supports reduced the electron cloud density of the Pd particles and weaken the adsorption of C-H, which affected the water resistance and stability of the Pd-based catalyst (Wang et al 2014). Our previous work indicated that phosphorous modified γ-Al_2O_3 nanosheet presented an enhanced both thermal stability of γ-Al_2O_3 and resistance to sintering of PdO_x, PdO_x supported P-modified Al_2O_3 calcined at 1000°C still exhibited a superior catalytic activity for propane combustion due to the re-dispersion of PdO_x particles and the SMSI at high temperature (Wu et al 2014). However, the surface modification of phosphorous led to the occupation of the coordinatively unsaturated Al^{3+} centers and the highly-active adsorption sites, which restrained the loading of Pd and the further enhancement of catalytic activity and stabilization of Pd species.

SiO_2 was doped in γ-Al_2O_3 as an inert component, it can not only inhibit the phase change of γ-Al_2O_3 at high temperature, but also avoid the weakening of the competitive adsorption of C-H by Pd particles caused by the doping of La (Mardkhe et al 2015). Here, Si was doped into Al_2O_3 by a dynamic hydrothermal method in the presence of tetrapropylammonium hydroxide (TPAOH), effects of Si on morphology and thermal stability of Al_2O_3 were firstly investigated. Al_2O_3 nanosheet was successfully synthesized, and the Si doping obviously thinned its thickness and improved the thermal stability. Sequentially, the synthesized Al_2O_3 nanosheet was used as support of PdO_x catalyst for catalytic combustion of propane, physicochemical properties of Pd/Si-Al_2O_3 nanosheets were characterized by XRD, H_2-TPR, XPS, CO pulses and in situ CO adsorption DRIFTS, and effects of Si content, high temperature aging and H_2O were investigated.

2. Experimental Section

2.1. Synthesis of Si doped Al_2O_3 nanosheets

A series of different contents of Si doped alumina nanosheets were prepared through a dynamic (60 rpm) hydrothermal method (Wu et al 2014). In a typical experiment, 2.5 g of polyethylene glycol with average molecular weight of 600 (PEG 600) and 0.902 g of sodium nitrate ($NaNO_3$, ≥ 99.0%) were dissolved in 54 ml of distilled water and stirred for 10 min. Then 15.3 g of tetrapropylammonium hydroxide solution (TPAOH, 25% in H_2O) and 3.12 g of aluminum isopropoxide (AIP, > 98%) were added to the mixture and stirred for 1 h, and next the given mass percentage of tetraethyl orthosilicate ($SiC_8H_{20}O_4$, liquid, 99.9%,

TEOS) was added dropwise, other Si sources such as sodium metasilicate, silica sol and water glass also were investigated and the expected Si content (SiO_2) was 3.6 wt.%. The mixed solution was stirred at room temperature for 24 h, and then transferred to a 100 mL polytetrafluoroethylene hydrothermal kettle and hydrothermally heated under dynamic conditions of 150 ºC (rotating at a speed of 60 rpm) for 48 h. Finally, the white precipitate was cooled to room temperature, filtered, washed, dried, and then calcined at 500, 800 or 1000 ºC for 4 h, respectively. The prepared Si doped Al_2O_3 nanosheets were marked as XSiAlNS-Y (X denoted the mass content of Si, Y meant the calcination temperature).

2.2. Preparation of supported palladium catalysts

The preparation of the XSiAlNS-500 supported Pd catalyst was achieved by an excessive impregnation method by adjusting the pH value of the impregnation solution. Specifically, 1 g of the calcined XSiAlNS-500 was ultrasonically dispersed in 200 mL of deionized water for 30 min, and HNO_3 was used to adjust the pH to 3 ~ 3.5. Then, 0.5 mL (the weight content of Pd was expected to be 1%) of palladium precursor (20 mg/mL H_2PdCl_4) was diluted in 200 mL of deionized water (pH = 3), and then was dropped into the XSiAlNS-500 suspension at a speed of 1 mL/min through a peristaltic pump. After stirring for 24 h the suspension was filtered, washed, dried and calcined at 500 or 800°C for 4 h. The prepared sample was remarked as Pd/XSiAlNS-500-T (T meant the calcination temperature).

2.3. Catalytic combustion of propane

The catalytic combustion reaction of propane was carried out in a continuous flow microreactor composed of U-shaped quartz tubes (inner diameter = 4 mm) under atmospheric pressure. 20 mg catalyst (60–80 mesh) was placed at the bottom of the reactor between the two layers of quartz wool. Then, the feed gas containing 0.1 vol.% C_3H_8, 20 vol.% O_2, and balanced with Ar was passed through the reactor at a flow rate of 50 mL/min with the gas hourly space velocity (GHSV) being 15,000 $ml \bullet g^{-1} \bullet h^{-1}$. The catalyst was ramped from 100 ℃ to 400 ℃ at the heating rate of 5 ℃/min, and composition of effluent gases were analyzed on-line by a gas chromatograph (GC-2060) equipped with a flame ionization detector (FID).

2.4. Characterization of the catalyst

The morphology of the catalyst was tested on a Hitachi S-3400N Scanning Electron Microscope (SEM), operating with an acceleration voltage of 15 kV. The powder X-ray diffraction patterns (XRD) were collected on a Bruker D8 Focus diffractometer with Cu Kα radiation (λ = 0.15406 nm, operated at 40 mA and 40 kV). The diffractograms were recorded within the 2θ range of 10 to 80° with a 2θ step size of 6° and a step time of 1 min. The specific surface area (S_{BET}) of the sample was tested by the Micromeritics ASAP 2020 analyzer. Before the test, the catalyst was pretreated in a vacuum environment at 200°C for 8 h, and then tested at -196°C. The specific surface area of the catalyst was obtained by the BET (Brunauer-Emmett-Teller) formula. The composition, content and valence of the surface elements of the catalyst were detected by ESCALAB 250 X-ray electron spectrometer. The X-ray source was monochromatic Al Kα palladium (1486.6 eV), and the binding energy was corrected by carbon C1s (284.8 eV).

The Pd dispersion was determined by CO pulses and tested on Autochem 2920 II chemical adsorption analyzer. First, the catalyst (50 mg) was reduced with 50 mL/min 10% H_2/N_2 mixture at 200 ℃ for 0.5 h, and then cooled to 30 ℃ in flowing He. Several pulses of CO were introduced until no more adsorption was observed. The Pd dispersion was calculated from the amount of CO chemisorption by assuming a stoichiometric ratio of CO/Pd = 1/1. H_2-TPR was detected by a TPDRO 1100 chemical adsorption apparatus equipped with a thermal conductivity detector (TCD). 10 vol% H_2/N_2 flow passed through 50 mg of sample at a flow rate of 40 mL/min, the temperature was ramped linearly from 30 ℃ to 500 ℃ at 10 ℃/min. The actual hydrogen consumption of the catalyst was calculated using the H_2 consumption of copper oxide as a reference.

In situ CO adsorption DRIFTS was detected on a Nicolet 6700 Fourier Transform Infrared Spectrometer with 64 scans and a resolution of 4 cm^{-1}. First, the catalyst (20 mg) was pretreated with 50 mL/min 20 vol.% O_2/Ar at 300 ℃ for 1 h, and then purged with 50 mL/min Ar at 150 ℃ for 0.5 h. After cooling down to room temperature and collecting background, CO adsorption was carried out under 50 mL/min 20 vol.% for 0.5 h.

3. Results And Discussion

3.1. Effect of Si doping on morphology and thermal stability of Al_2O_3 nanosheet

Figure 1 showed SEM images of Si doped Al_2O_3 with different Si sources and different Si doping amounts, it can be found that all synthesized Al_2O_3 presented three-dimensional flower-like structures assembled by nanosheets and the doping of Si did not destroy the morphology of Al_2O_3 (Wu et al 2014). However, the thickness of Al_2O_3 nanosheets varied as different Si sources (3.6 wt.% Si). The thickness of the prepared nanosheet without adding Si was about 80 nm, while the addition of TEOS or sodium metasilicate (Na_2SiO_3) significantly reduced the thickness of Al_2O_3 nanosheets and the average thickness was about 30 nm **(**Fig. 1c **and f)**. When Silica sol and water glass were used as Si sources, the average thickness of Al_2O_3 nanosheets was about 60 nm **(**Fig. 1a **and b)**. Our previous work (Wu et al 2014) indicated that Al_2O_3 nanosheets with regular leaf-like architecture could be synthesized by a novel intercalation-swelling-exfoliation pathway and then its morphology/thickness could be further adjusted via the dissolution-growth induced by phosphate. Here, similar roles of the Si with phosphate were observed. Sequentially, the effect of Si content using TEOS as Si source was investigated and showed in Fig. 1d-h. It can be found that the thickness of Al_2O_3 nanosheets obviously thinned with the increase of the Si content, for examples, the thickness of 0SiAlNS-500 and 1.8SiAlNS-500 was about 100 nm and 70 nm, while the thickness of the 3.6-7.2SiAlNS-500 samples drastically decreased to about 30 nm. Additionally, the morphology of Al_2O_3 nanosheets also varied with the Si content, an evolution from irregular nanosheets of 0SiAlNS-500 and 1.8SiAlNS-500 to the flower-like architecture assembled by

regular leaf-like nanosheets of the 3.6-7.2SiAlNS-500 samples was observed, but too much Si (7.2 wt.% Si) would lead to the accumulation of the leaf-like nanosheets.

Effect of Si content on thermal stability of synthesized Al_2O_3 nanosheets was further investigated by XRD and specific surface area of the samples calcined at different temperatures, and the results were listed Fig. 2. XRD patterns shown in Fig. 2 illustrated that the crystal phase of XSiAlNS-Y evolved in the sequence of γ→δ→θ→α in the ranges of 500 and 1200°C but the characteristic peaks of SiO_2 appeared when the content of Si increased to 7.2 wt.% (7.2SiAlNS-Y). In particular, all 0SiAlNS-Y and 3.6SiAlNS-Y samples only presented a γ phase after calcined at 500°C or 800°C, with the further increasing of the calcined temperature to 1000 and 1200°C, the phase of 0SiAlNS-Y transformed into θ- and α-phase while the γ phase was still maintained after calcining at 1000°C for 3.6SiAlNS-Y and 7.2SiAlNS-Y samples and only θ phase formed even at 1200°C (α-phase was not observed). Thereby, XRD results showed that Si doping effectively suppressed the high-temperature phase transformation of Al_2O_3 nanosheets and enhanced its thermal stability, which attributed to the fact that Si occupied the holes of the AlO_4 tetrahedron in Al_2O_3 and inhibited the O^{2-} reconstruction to hcp (Mardkhe et al 2015). Meanwhile, the presence of SiO_2 could isolate Al_2O_3 particles and prevent its aggregation. Additionally, the specific surface area of the XSiAlNS-Y calcined at different temperatures was determined. The 3.6SiAlNS sample presented a better resistance to sintering and the specific surface area still up to 100.5 and 56.3 $m^2 \bullet g^{-1}$ after calcining at 1000°C and 1200°C, respectively, while the specific surface area of the 0SiAlNS-1000 and 0SiAlNS-1200 samples decreased from 64.2 $m^2 \bullet g^{-1}$ sharply to 20.1 and 12.8 $m^2 \bullet g^{-1}$. This result further confirmed that the doping of Si improved the thermal stability of Al_2O_3 nanosheets, which was critical in catalysis reactions occurred at high temperature.

3.2. Characterization of Pd supported on Al_2O_3 nanosheets

Al_2O_3 nanosheets (XSiAlNS-500) with different Si content calcined at 500°C were further investigated as supports of Pd and its physicochemical properties were evaluated. Figure 2e and 2f showed XRD patterns of Pd supported on Al_2O_3 nanosheets. Only γ phase Al_2O_3 was detected in all samples and no characteristic diffraction peaks of PdO or Pd appeared even after calcining at 800°C, indicating that Pd presented a high dispersion on Al_2O_3 nanosheets surface. Interestingly, it can be observed from Fig. 2a-b and 2e-f that the peaks corresponding to SiO_2 phase of the Pd supported on 7.2SiAlNS catalysts disappeared, which indicated that the surface SiO_2 was re-doped into the defective spinel structure of γ-Al_2O_3 during the secondary calcination process, or the partial etching of Si residue on Al_2O_3 surface occurred due to the low pH value (about 3.0) during the loading of Pd.

Table 1
The Pd content of the Pd/XSiAlNS-500-T catalysts, as well as T_{90} and reaction rate (r, at 225°C) for C_3H_8 combustion

Catalyst	Pd particle size (nm)[a]	Pd dispersion (%)[b]	T_{90} (°C)	$r \times 10^7$ (mol/g/s)[c]	E_a (kJ/mol)
Pd/0SiAlNS-500-500	13	11.6	280	106	80.8
Pd/3.6SiAlNS-500-500	4.3	34.3	278	371	72.4
Pd/7.2SiAlNS-500-500	4.6	37.2	282	205	80.2
Pd/0SiAlNS-500-800	19	4.1	302	111	82.6
Pd/3.6SiAlNS-500-800	9.7	16.6	278	242	94.8
Pd/7.2SiAlNS-500-800	5.2	35.7	278	205	101.4
[a] Detected by HRTEM.					
[b] Calculated based on CO chemisorption at 30 ℃.					
[c] at 225 ℃.					

The states of Pd on Al_2O_3 nanosheets such as particle size, dispersion, valence and redox ability were further characterized by HRTEM, CO pulse, CO-DRIFT, XPS and H_2-TPR. HRTEM images in Fig. 3 indicated that the doping of Si obviously reduced the size of Pd particles and promoted its dispersion. The average particle size (Table 1) decreased from 13 nm (Pd/0SiAlNS-500-500) to 4.3 nm (Pd/3.6SiAlNS-500-500) and 4.6 nm (Pd/7.2SiAlNS-500-500). Moreover, HRTEM images of the Pd supported catalysts at 800°C revealed that the size of Pd particles in the Pd/0SiAlNS-500-800 and Pd/3.6SiAlNS-500-800 catalysts increased from 13 and 4.3 nm to 19 and 9.7 nm while the sintering of Pd particles in Pd/7.2SiAlNS-500-800 was not observed, which implied that the introduction of Si not only enhanced the thermal stability of Al_2O_3 but also improved the resistance to Pd sintering. An isolation effect of SiO_2 was responsible for the better resistance to sintering of Pd/7.2SiAlNS, since a small portion of SiO_2 (when the high content of SiO_2 was doped) aggregated to form SiO_2 phase and migrated to the Al_2O_3 surface at high temperature and prevented the intergranular sintering of PdO_x (Dai et al 2018). Additionally, as shown in Table 1, the CO pulse tests further confirmed that a higher Pd dispersion was observed on Si doped Al_2O_3 nanosheets, and the sintering of Pd particles also was suppressed and more significant with the increasing of Si content.

Figure 4a-b displays IR spectra of CO adsorption (CO-DRIFT) on Pd/XSiAlNS-500-T catalysts. Based on the intensity of CO adsorption peaks, it can be found that the adsorption of CO on Pd/0SiAlNS catalysts was notably less than that on Si doping Al_2O_3 nanosheets, which was attributable to the lower Pd dispersion (HRTEM and CO pulse). Moreover, some obvious differences in wavenumber and the number of adsorption peaks were observed, Pd/0SiAlNS-500-500 catalyst mainly showed two CO adsorption peaks at 2115 cm^{-1} and 2087 cm^{-1}, which were attributed to the linear adsorption of CO on $Pd^{\sigma+}(0 < \sigma < 1)$ and Pd^0 (Murata et al 2017); while the CO adsorption peaks on Si doped catalysts shifted to the high wavenumber (up to 2139 cm^{-1}) besides the peak at 2086 cm^{-1}, which were attributed to the linear adsorption of CO on Pd^+ (Pd with higher valence) (Dai et al 2018). These results indicated that the high Pd dispersion was confirmed (HRTEM and CO pulse) and the doping of Si led to the Pd electrons transfer to Si or suppressed the reduction of PdO_x by CO. In addition, some weak bands at 1976, 1962, 1924 and 1930 cm^{-1} assigned to the bridged adsorption of CO on PdO_x, and the bands at 1976 and 1962 cm^{-1} corresponding to the adsorption of CO on the stepped PdO_x were also observed (Jbir et al 2016). For all the samples aged at 800°C, the intensity of bands decreased compared with fresh samples, which may be caused by the sintering of the Pd particles or the disappearance of the corners and edges of the Pd particles (Ding et al 2016), and consistent with HRTEM and CO pulse results. Moreover, it could be found that the bands at high wavenumber on the aged sample disappeared, corresponding to higher valence Pd species, which was probably attributed to the decomposition of PdO_x at high temperature. Specifically, the CO linear adsorption of the Pd/7.2SiAlNS-500-800 (2092 cm^{-1}) and Pd/0SiAlNS-500-800 (2069 cm^{-1}) samples were mainly located in the range of the Pd^0-CO characteristic adsorption peak (2060–2100 cm^{-1}) (Dai et al 2018); however, the main CO linear adsorption band of the Pd/3.6SiAlNS-500-800 sample was at 2127 cm^{-1} with a weaker linear adsorption peak of 2022 cm^{-1} (attributed to the smaller Pd nanoparticles with lower electron density) (Rades et al 1996).

The Pd 3d XPS spectra of the Pd/XSiAlNS-500-T catalyst were showed in Fig. 4c-d. The characteristic peaks assigning to Pd^{2+} at 336.4, 336.5, 336.6 and 336.8 eV were observed on all catalysts and independent of the Si content and calcination temperature (Kusumawati et al 2019). The Pd^0 was not detected, which indicated that Pd^0 species determined by CO-DRIFT was possibly ascribed to the reduction of PdO_x by CO due to the good redox ability of the supported PdO_x (Hoflund et al 2003). Therefore, the redox performance of Pd/XSiAlNS-500-T catalysts was evaluated by H_2-TPR and shown in Fig. 5. For all the Pd/XSiAlNS-500-500 catalysts, the reduction peak was not observed but a negative peak attributing to the decomposition of PdH_x species appeared at 60–80 ℃, which indicated that PdO_x species had been easily reduced at low temperature (at 40 ℃) due to the high dispersion of PdO_x. However, the peak temperature and intensity were varied with the Si content. Specifically, the amount of PdH_x species (the intensity of the negative peak) decreased with the increase of Si content, which was attributed to the smaller formation enthalpy of PdH_x when H atoms combined with Pd in the bulk phase (Delogu et al 2010). In addition, the highest decomposition temperature of PdH_x in the Pd/3.6SiAlNS-500-500 sample also proved that the particle size of the Pd/0SiAlNS-500-500 sample was relatively large,

which was consistent with the TEM results. However, it can be observed that the lower decomposition temperature of the Pd/7.2SiAlNS-500-500 sample was caused by the reduction of the metal-support interaction caused by the Si on the surface (Murata et al 2017; He et al 2003). After Pd/XSiAlNS catalysts were aged at 800 ℃, obvious differences were observed compared with the fresh catalysts. Pd/0SiAlNS-500-800 and Pd/7.2SiAlNS-500-800 catalysts presented a reduction peak at about 60 ℃, while only a negative peak from the decomposition of PdH_x species on Pd/3.6SiAlNS-500-800 catalyst was detected. The results revealed that the former two were more difficult to be reduced, but might be ascribed to different factors. For the Si undoped Al_2O_3, the obvious sintering and aggregation of PdO_x particles due to the weak metal-support interaction was the dominant factor, while the encapsulation and segregation of PdO_x particles owing to the migrated SiO_2 to the surface of Al_2O_3 was responsible for the more difficult reduction of Pd/7.2SiAlNS-500-800 (the sintering of PdO_x particles at high temperature was not observed) (Nampi et al 2010).

3.4. Catalytic Combustion of Propane

The catalytic performance of Pd/XSiAlNS-500-T catalysts was investigated through catalytic combustion of propane, and Fig. 6 displays its light-off curves under the conditions of 0.1% C_3H_8 and 20% O_2 in Ar at a space velocity of 15,000 $ml \bullet g^{-1} \bullet h^{-1}$. Almost silent effect on catalytic activity was observed and T_{50} (the temperature achieved 50% conversion of C_3H_8) of all the Pd/XSiAlNS-500-500 catalysts was about 226 ℃ **(**Fig. 6b**).** It is meaningful for Pd decorated Al_2O_3 catalysts because the presence of trace Si in Al_2O_3 generally was considered to be poisoning to supported noble metals such as three-way catalysts (TWCs) for the control of vehicle exhaust pollution,[40] which was possibly ascribed to the high dispersion of PdO_x particles due to the isolation effect of Si (the pH value of the impregnating solution was adjusted to 3.0, lower than the isoelectric point of Al_2O_3 but higher than the isoelectric point of SiO_2, thus Pd was considered to be preferentially adsorbed on Al_2O_3). However, for the aged catalysts at 800°C (Pd/XSiAlNS-500-800), the doping of Si evidently inhibited the declining of activity and presented a better resistance-sintering of high temperature, the T_{90} of Pd/3.6SiAlNS-500-800 and Pd/7.2SiAlNS-500-800 was equivalent to that of the fresh catalysts while the T_{90} of Pd/0SiAlNS-500-800 increased from 280 to 302°C. Table 1 clearly indicated that the doping of Si suppressed the aggregation of PdO_x particles. Nevertheless, when considering the T_{50} (Fig. 6b), the high temperature aging caused the slight loss of activity of Pd supported Si-doped Al_2O_3 catalysts and T_{50} increased by 4–10°C, but Pd/3.6SiAlNS still presented the best performance (only increasing of 4°C) while Pd supported pristine Al_2O_3 catalyst increased by 30°C. In short, the doping of Si did not suppress catalytic activity of Pd/γ-Al_2O_3 catalysts instead promoted the resistance-sintering, which was attributed to the high dispersion of the PdO_x particles and the improvement of the thermal stability of Al_2O_3 due to the Si doping. However, it should be noted that performances of Pd/γ-Al_2O_3 catalysts were not continuedly improved after the much Si was doped (Pd/7.2SiAlNS), because the introduction of much Si led to the formation of SiO_2 phase, which could prevent the aggregation of PdO_x particles but also weaken the interaction between the PdO_x

particles and the Al_2O_3 support, and then brought the intergranular sintering of the PdO_x particles (Dai et al 2018).

Effects of H_2O on catalytic combustion of propane (catalytic activity and stability) over Pd/XSiAlNS-500-500 catalysts were comparatively investigated, and the results are showed in Fig. 7. The presence of H_2O obviously suppressed catalytic combustion of propane on all catalysts, which was ascribed to the competitive adsorption of propane and H_2O on PdO_x active sites or the transformation of the instable PdO_x into $Pd(OH)_x$ (Goodman et al 2017). More importantly, it could be found that the doping of Si enhanced the water-resistance of Pd/Al_2O_3 catalysts especially for Pd/3.6SiAlNS-500-500. For example, T_{90} of the Pd/0SiAlNS-500-500 increased by 73 ℃ (from 278 ℃ to 351 ℃) while T_{90} of Pd/3.6SiAlNS-500-500 (from 278 ℃ to 322 ℃) only increased by 45 ℃. It could be speculated that the increasing of the hydrophobicity and stabilization of PdO_x particles (the strong interaction between PdO_x and Si doped Al_2O_3) was responsible for the better water-resistance of Si doped catalysts. Additionally, Pd/7.2SiAlNS-500-500 presented an almost overlapping light-off curve with Pd/3.6SiAlNS-500-500 in the range of lower temperature, but the propane conversion over Pd/7.2SiAlNS-500-500 catalyst was slightly below that of Pd/3.6SiAlNS-500-500 as the temperature increased and T_{90} increased from 322 ℃ to 341 ℃. The aged experiments and the corresponding characterization results confirmed that the PdO_x particles on the Pd/3.6SiAlNS-500-500 catalyst showed a better stability, thus the deactivation from the transformation of the instable PdO_x into $Pd(OH)_x$ was more restrained. Additionally, the prolonged stability of Pd/XSiAlNS-500-500 catalysts for catalytic combustion of propane under the alternate dry and humid conditions (3 vol.% H_2O) at 300 ℃ were evaluated and showed in Fig. 7b. The three catalysts presented almost same conversion of propane under dry conditions. After 3 vol.% H_2O was introduced, the conversion of propane rapidly declined but differences in these catalysts. The doping of Si retarded the inhibition of H_2O on catalytic combustion of propane and Pd/3.6SiAlNS-500-500 still presented the highest catalytic activity, which was consistent with the results from activity tests. More importantly, the conversion of propane could quickly restore the initial conversion and even a higher conversion (from 86–96%) was detected on Pd/3.6SiAlNS-500-500 after H_2O was switch off, which indicated that the effect of H_2O was reversible. Even after running for 50 h, only a slight deactivation of Pd/0SiAlNS-500-500 (from 85–82%) and Pd/7.2SiAlNS-500-500 (from 89–88%) catalysts was observed, while the Pd/3.6SiAlNS-500-500 catalyst still presented an increased conversion of propane by 10% (from 86–96%). The results re-confirmed that the doping of Si improved the water-resistance of the supported Pd catalyst, and the activity promotion of Pd/3.6SiAlNS-500-500 was considered to be related with the possible redispersion of PdO_x with high stability and SMSI in the presence of H_2O (Nie et al 2017; Zhao et al 2017).

4. Conclusions

The Si-doped Al_2O_3 nanosheets were synthesized by a dynamic hydrothermal method in the presence of TPAOH as precipitating and swelling agent. The influence of different Si sources and Si doping amounts on the structure of alumina was investigated, and it was found that TEOS precursor could significantly

tune the thickness of the Al_2O_3 nanosheets and reduced from 80 nm to 30 nm when the 3.6% Si was doped. Moreover, the doping of Si improved the thermal stability of Al_2O_3 nanosheets. The θ phase was still maintained after calcination and even the specific surface area was as high as 56.3 $m^2 \bullet g^{-1}$ at 1200 ℃. Sequentially, the supported Pd catalysts using the Si doped Al_2O_3 nanosheets as supports were prepared by an excessive impregnation method with a tailoring pH value. Characterizations results of HRTEM, CO pulse and CO-DRIFT indicated that the doping of Si increased the dispersion of Pd and the formation of stabilized PdO_x particles, while the increase in Si doping (7.2%) caused the aggregation of Si to form SiO_2 segregation, weakening the SMSI and leading to the poor dispersion of Pd. Catalytic combustion of propane as typical model reaction for the purification of industrial VOCs and automobile hydrocarbon emissions revealed that the appropriate Si doping (3.6%) promoted the resistance-sintering and water-resistance of the supported Pd catalysts, which was attributed to the preferable SMSI, the high dispersion of the PdO_x particles and the improvement of the thermal stability of Al_2O_3 due to the Si doping.

Declarations

Acknowledgment

This work was supported by the National Key Research and Development Program of China (No. 2016YFC0204300), National Natural Science Foundation of China (No. 21922602, 21777043, 22076047), and Natural Science Foundation of Shanghai (19ZR1412900). Additional support was provided by Fundamental Research Funds for the Central Universities.

Author's contribution

Mingxiang Jiang: Investigation, Methodology, Writing - original draft. Qingqing Wu: Investigation, Methodology, Validation, Writing - review & editing. Jiaorong Yan: Formal analysis, Writing - review & editing. Jun Pan: Supervision, Formal analysis, Writing - review & editing. Qiguang Dai: Supervision, Formal analysis, Writing - review & editing. Wangcheng Zhan: Supervision, Funding acquisition, Writing - review & editing.

Data availability

The datasets used and/or analysed during the current study are available from the corresponding author on reasonable request.

Compliance with ethical standards

Ethics approval and consent to participate

Not applicable.

Consent for publication

Not applicable.

Conflict of interest

The authors declare that they have no known competing financial interests or personal relationships that could have appeared to influence the work reported in this paper.

References

1. Busca G (2014) The surface of transitional aluminas: A critical review. Catal Today 226:2–13. http://dx.doi.org/10.1016/j.cattod.2013.08.003
2. Cargnello M, Delgado JJ et al (2012) Exceptional Activity for Methane Combustion over Modular Pd@CeO_2 Subunits on Functionalized Al_2O_3. Science 337:713–717. http://dx.doi.org/10.1126/science.1222887
3. Chen B, Lin J et al (2019) Cooperative Catalysis of Methane Oxidation through Modulating the Stabilization of PdO and Electronic Properties over Ti-Doped Alumina-Supported Palladium Catalysts. ACS Omega 4:18582–18592. http://dx.doi.org/10.1021/acsomega.9b02370
4. Cai T, Deng W et al (2020) Great activity enhancement of Co_3O_4/γ-Al_2O_3 catalyst for propane combustion by structural modulation. Chem Eng J 395:125071. https://doi.org/10.1016/j.cej.2020.125071
5. Dai Q, Zhu Q, Lou Y, Wang X (2018) Role of Brønsted acid site during catalytic combustion of methane over PdO/ZSM-5: Dominant or negligible. J Catal 357:29–40. https://doi.org/10.1016/j.jcat.2017.09.022
6. Dai Y, Lu P, Cao Z, Campbell CT, Xia Y (2018) The physical chemistry and materials science behind sinter-resistant catalysts. Chem Soc Rev 47 (2018) 4314–4331. https://doi.org/10.1039/c7cs00650k
7. Delogu F (2010) Smooth Size Effects in Pd and PdH_x Nanoparticles. J Phys Chem C 114:18085–18090. https://doi.org/10.1021/jp106182n
8. Ding L, Yi H et al (2016) Activating Edge Sites on Pd Catalysts for Selective Hydrogenation of Acetylene via Selective Ga_2O_3 Decoration. ACS Catal 6:3700–3707. https://doi.org/10.1021/acscatal.6b00702
9. Fang R, Cui Y et al (2015) Promotion of a Pd/Al_2O_3 close-coupled catalyst by Ni. Chin J Catal 36:994–1000. https://doi.org/10.1016/S1872-2067(15)60850-6
10. Goodman ED, Dai S et al (2017) Mechanistic Understanding and the Rational Design of SinterResistant Heterogeneous Catalysts. ACS Catal 7:4372–4380. . 10.1021/acscatal.7b01975
11. Han D, Wang Z, Cheng J et al (2017) Volatile organic compounds (VOCs) during non-haze and haze days in Shanghai: characterization and secondary organic aerosol (SOA) formation. Environ Sci Pollut Res 24:18619–18629. https://doi.org/10.1007/s11356-017-9433-3
12. He C, Cheng J, Zhang X et al (2019) Recent Advances in the Catalytic Oxidation of Volatile Organic Compounds: A Review Based on Pollutant Sorts and Sources. Chem Rev 119:4471–4568.

https://doi.org/10.1021/acs.chemrev.8b00408

13. He C, Shen Q, Liu M (2014) Toluene destruction over nanometric palladium supported ZSM-5 catalysts: influences of support acidity and operation condition. J Porous Mater 21:551–563. https://doi.org/10.1007/s10934-014-9802-y
14. Hoflund GB, Hagelin HAE, Weaver GF, Salaita GN (2003) ELS and XPS study of Pd/PdO methane oxidation catalysts. Appl Surf Sci 205:102–112. https://doi.org/10.1016/S0169-4332(02)01084-X
15. Hu Z, Wang Z, Guo Y, Wang L, Zhang J, Zhan W (2018) Total Oxidation of Propane over a Ru/CeO_2 Catalyst at Low Temperature Environ. Sci Technol 52:9531–9541. https://doi.org/10.1021/acs.est.8b03448
16. Jing Y, Cai Z et al (2019) Promotional Effect of La in the Three-Way Catalysis of La-Loaded Al_2O_3–Supported Pd Catalysts ($Pd/La/Al_2O_3$). ACS Catal 10:1010–1023. http://dx.doi.org/10.1021/acscatal.9b03766
17. Jbir I, Couble J et al (2016) Individual Heat of Adsorption of Adsorbed CO Species on Palladium and Pd – Sn Nanoparticles Supported on Al_2O_3 by Using Temperature-Programmed Adsorption Equilibrium Methods. ACS Catal 6:2545–2558. https://doi.org/10.1021/acscatal.5b02749
18. Khairudin NF, Mohammadi M (2021) An investigation on the relationship between physicochemical characteristics of alumina-supported cobalt catalyst and its performance in dry reforming of methane. Environ Sci Pollut Res. https://doi.org/10.1007/s11356-021-12794-0
19. Kusumawati EN, Sasaki T (2019) Highly active and stable supported Pd catalysts on ionic liquid-functionalized SBA-15 for Suzuki–Miyaura cross-coupling and transfer hydrogenation reactions. Green Energy Environ 4:180–189. https://doi.org/10.1016/j.gee.2019.02.003
20. Lai CH, Chang CC, Wang CH et al (2009) Emissions of liquefied petroleum gas (LPG) from motor vehicles. Atmos Environ 43:1456–1463. https://doi.org/10.1016/j.atmosenv.2008.11.045
21. Lin B, Wang A, Guo Y, Ding Y, Zhan W, Wang L, Guo Y, Gao F (2020) Appl Catal B Environ 279:119404. https://doi.org/10.1016/j.apcatb.2020.119404
22. Liu Q, Wang CL et al (2009) Dry citrate-precursor synthesized nanocrystalline cobalt oxide as highly active catalyst for total oxidation of propane. J Catal 263:104–113. https://doi.org/10.1016/j.jcat.2009.01.018
23. Liu Y, Deng J, Xie S, Wang Z, Dai H (2016) Organic emissions profile for a light-duty diesel vehicle. Chin J Catal 37:1193–1205. https://doi.org/10.1016/S1872-2067(16)62457-9
24. Liu Z, Cheng L et al (2020) Synthesis, characterization and catalytic performance of nanocrystalline Co_3O_4 towards propane combustion: Effects of small molecular carboxylic acids. J Solid State Chem 292:121712. https://doi.org/10.1016/j.jssc.2020.121712
25. Mardkhe MK, Huang B et al (2015) Synthesis and characterization of silica doped alumina catalyst support with superior thermal stability and unique pore properties. J Porous Mater 23:475–487. https://doi.org/10.1007/s10934-015-0101-z

26. Mohammad R, Badii K, Faghihi M, Sanati M, Cruise N, Augustsson O (2010) Catalysis: Volume. In: Spivey J, Roberts GW (eds) Deactivation of Oxidation Catalysts for VOC Abatement by Si and P Compounds, 17 edn. RSC-Publishing pp 210–257. https://doi.org/10.1039/9781847553294-00210
27. Murata K, Mahara Y et al (2017) The Metal–Support Interaction Concerning the Particle Size Effect of Pd/Al_2O_3 on Methane Combustion Angew. Chem Int Ed 56:15993–15997. https://doi.org/10.1002/anie.201709124
28. Nampi PP, Moothetty P, Berry FJ, Mortimer M, Warrier KG (2010) Aluminosilicates with varying alumina–silica ratios: synthesis via a hybrid sol–gel route and structural characterization. Dalton Trans 39:5101–5107. https://doi.org/10.1039/C001219J
29. Nie L, Mei D et al (2017) Activation of surface lattice oxygen in single-atom Pt/CeO_2 for low-temperature CO oxidation. Science 358:1419–1423. https://doi.org/10.1126/science.aao2109
30. Okal J, Zawadzki M (2009) Catalytic combustion of butane on $Ru/\gamma\text{-}Al_2O_3$ catalysts. Appl Catal B Environ 89:22–32. https://doi.org/10.1016/j.apcatb.2008.11.024
31. Ozawa M, Nishio Y et al (2016) Thermal stability and microstructure of catalytic alumina composite support with lanthanum species. Appl Surf Sci 380:288–293. http://dx.doi.org/10.1016/j.apsusc.2015.12.246
32. Rades T, Borovkov V et al (1996) Diffuse Reflectance IR Study of CO Adsorption on a Bimetallic Pt-Pd Catalyst Supported on NaY Zeolite. Evidence of Alloy Formation. J Phys Chem 100:16238–16241. https://doi.org/10.1021/jp9606063
33. Rahmati M, Safdari MS, Fletcher TH, Argyle MD, Bartholomew CH (2020) Chemical and Thermal Sintering of Supported Metals with Emphasis on Cobalt Catalysts During Fischer – Tropsch Synthesis. Chem Rev 120:4455–4533. https://dx.doi.org/10.1021/acs.chemrev.9b00417
34. Rahman MA (2019) Induction of hydrogen, hydroxy, and LPG with ethanol in a common SI engine: a comparison of performance and emission characteristics. Environ Sci Pollut Res 26:3033–3040. https://doi.org/10.1007/s11356-018-3861-6
35. Siegl W, Hammerle R, Herrmann H, Herrmann B, Wenclawiak B, Luers-Jongen B (1999) Organic emissions profile for a light-duty diesel vehicle. Atmos Environ 33:797–805. https://doi.org/10.1016/S1352-2310(98)00209-X
36. Wang J, Chen H, Hu Z, Yao M, Li Y (2014) A Review on the Pd-Based Three-Way Catalyst. Catal Rev 57:79–144. https://doi.org/10.1080/01614940.2014.977059
37. Wang Z, Huang Z, Brosnahan GT, Zhang S, Guo Y, Wang L, Wang Y, Zhan W (2019) Ru/CeO_2 Catalyst with Optimized CeO_2 Support Morphology and Surface Facets for Propane Combustion. Environ Sci Technol 53:5349–5358. https://doi.org/10.1021/acs.est.9b01929
38. Wu Q, Yan J, Jiang M, Dai Q, Wu J, Ha MN, Ke Q, Wang X, Zhan W (2014) Phosphate-assisted synthesis of ultrathin and thermally stable alumina nanosheets as robust Pd support for catalytic combustion of propane. Appl Catal B Environ 286:119949. https://doi.org/10.1016/j.apcatb.2021.119949

39. Yang X, Li Q, Lu E, Wang Z, Gong X, Yu Z, Guo Y, Wang L, Zhan W, Zhang J, Dai S (2019) Taming the stability of Pd active phases through a compartmentalizing strategy toward nanostructured catalyst supports. Nat Commun 10:1611. https://doi.org/10.1038/s41467-019-09662-4
40. Zhan YY, Kang L et al (2019) Pd/Al_2O_3 catalysts modified with Mg for catalytic combustion of methane: Effect of Mg/Al mole ratios on the supports and active PdO_x formation. J Fuel Chem Technol 47:1235–1244. https://doi.org/10.1016/S1872-5813(19)30050-7
41. Zhao S, Chen F et al (2017) Remarkable active-site dependent H_2O promoting effect in CO oxidation. Nat Commun 10:3824. https://doi.org/10.1038/s41467-019-11871-w
42. Zheng X, Chen X et al (2016) Total oxidation of VOCs on mesoporous iron oxide catalysts: Soft chemistry route versus hard template method. Chem Eng J 297:148–157. http://dx.doi.org/10.1016/j.cej.2015.12.109
43. Zhou R, Xing F et al (2014) CO and C_3H_8 total oxidation over Pd/La-Al_2O_3 catalysts: Effect of calcination temperature and hydrothermal treatment. J Rare Earths 32:621–627. http://dx.doi.org/10.1016/S1002-0721(14)60117-4

Figures

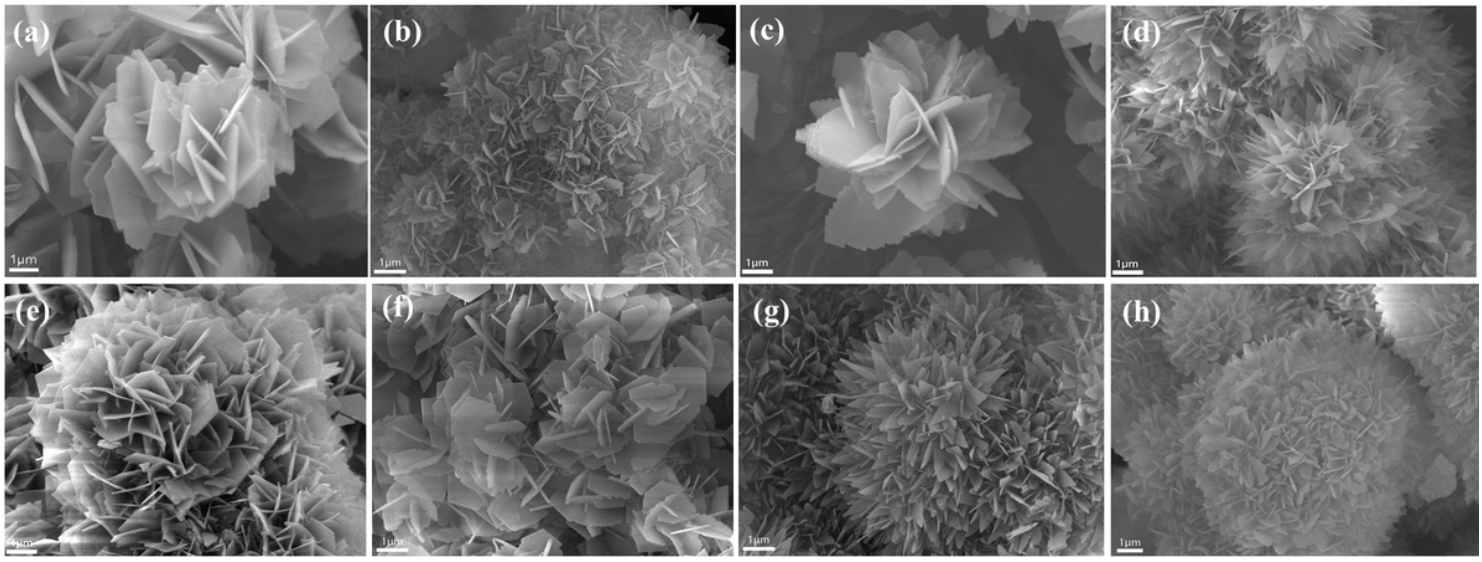

Figure 1

SEM images of the alumina samples prepared with different Si sources and Si content: without Si-doping (a), TEOS (b), Silica sol (c), water glass (d), Na2SiO3 (e), 1.8 wt.% TEOS (f), 5.4 wt.% TEOS (g), 7.2 wt.% TEOS (h)

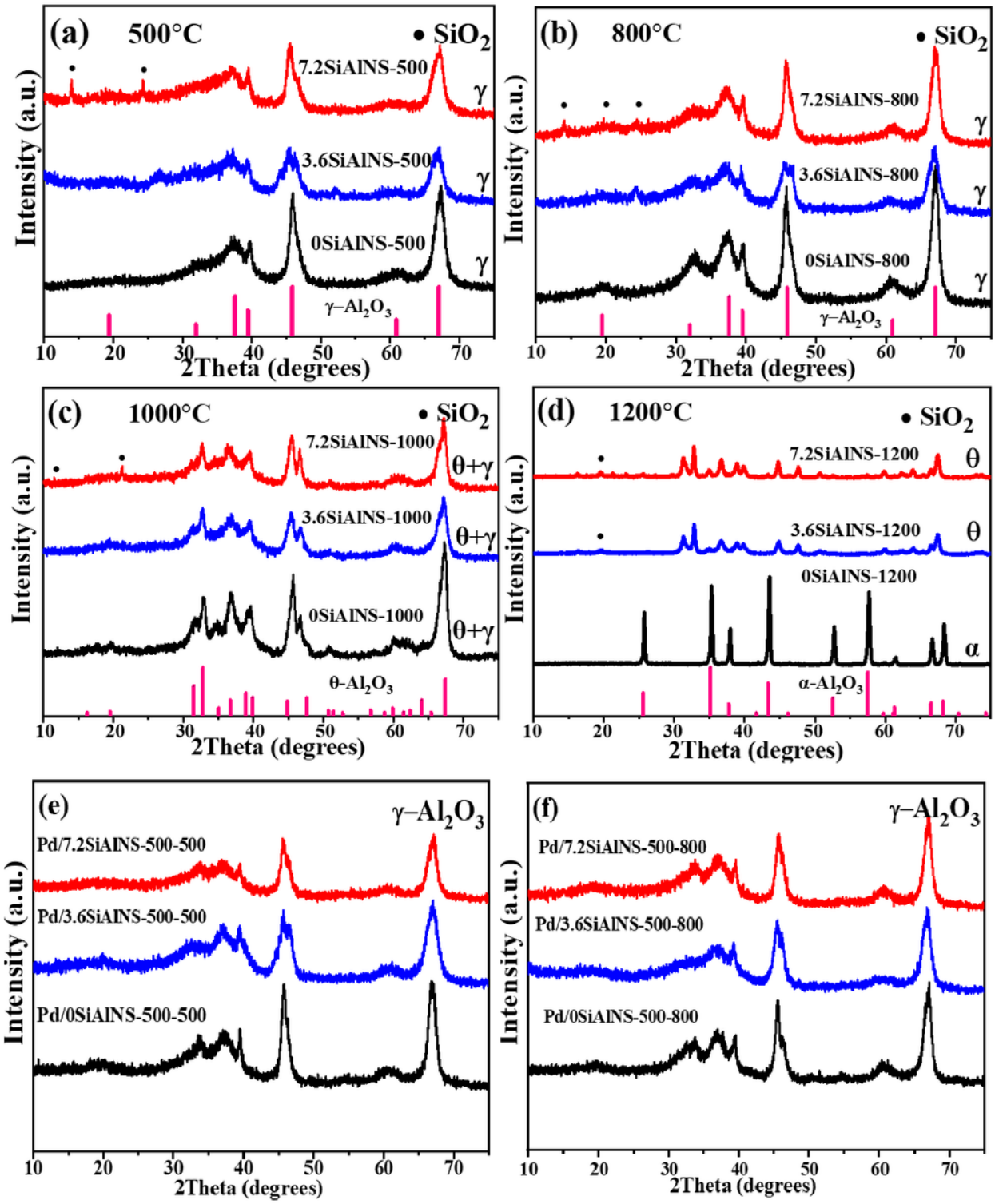

Figure 2

XRD patterns of Al2O3 nanosheets with different Si contents and Al2O3 supported Pd catalysts calcined at different temperatures

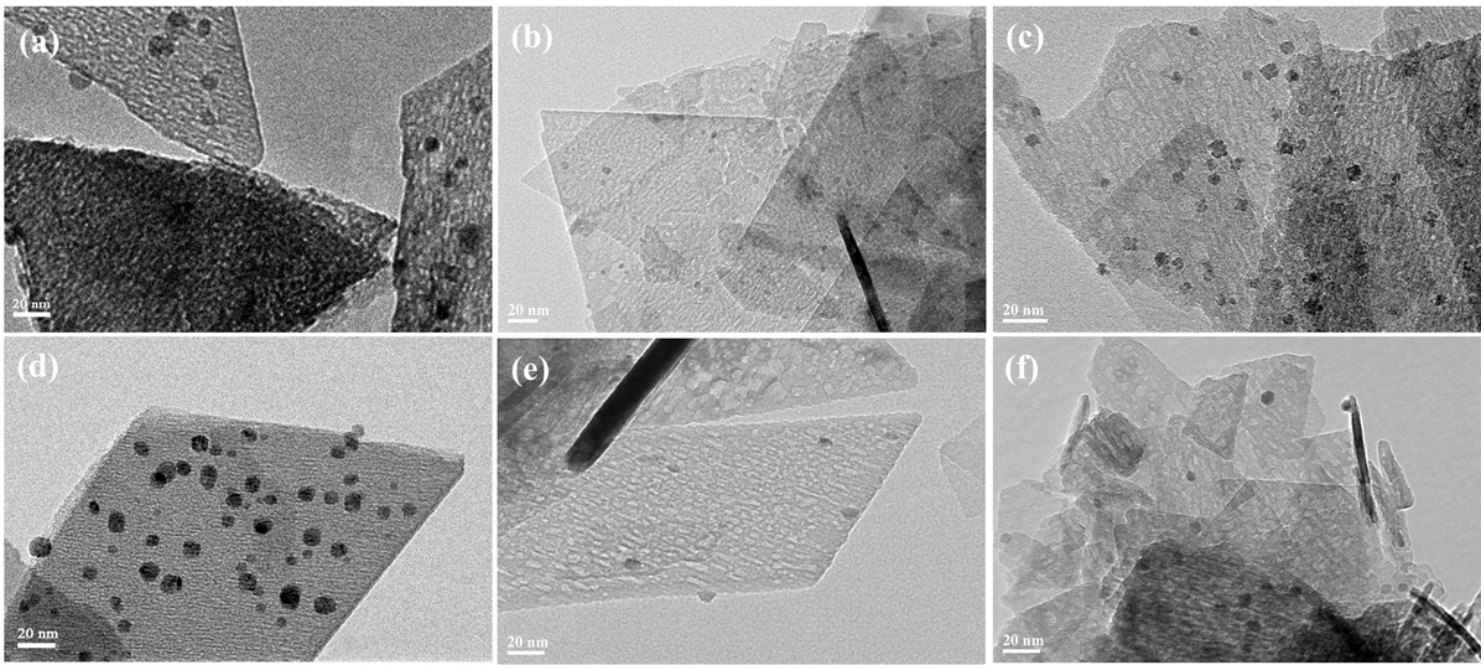

Figure 3

TEM images of Pd/0SiAlNS-500-500 (a), Pd/3.6SiAlNS-500-500 (b), Pd/7.2SiAlNS-500-500 (c), Pd/0SiAlNS-500-800 (d), Pd/3.6SiAlNS-500-800 (e), and Pd/7.2SiAlNS-500-800 (f)

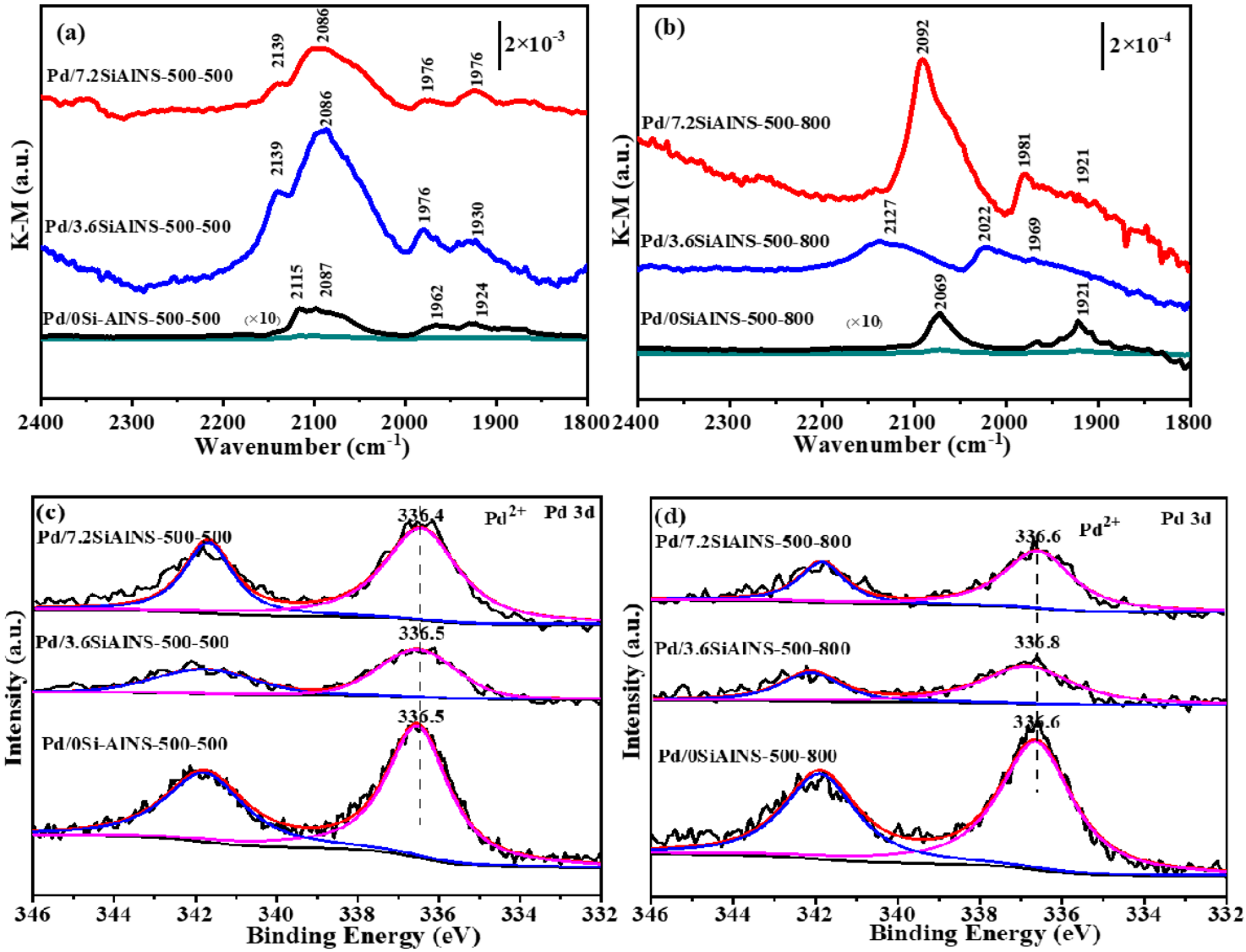

Figure 4

IR spectra of CO adsorption and Pd 3d XPS spectra of the Pd/XSiAlNS-500-T catalysts calcined at different temperature: 500 °C (a, c) and 800 °C (b, d)

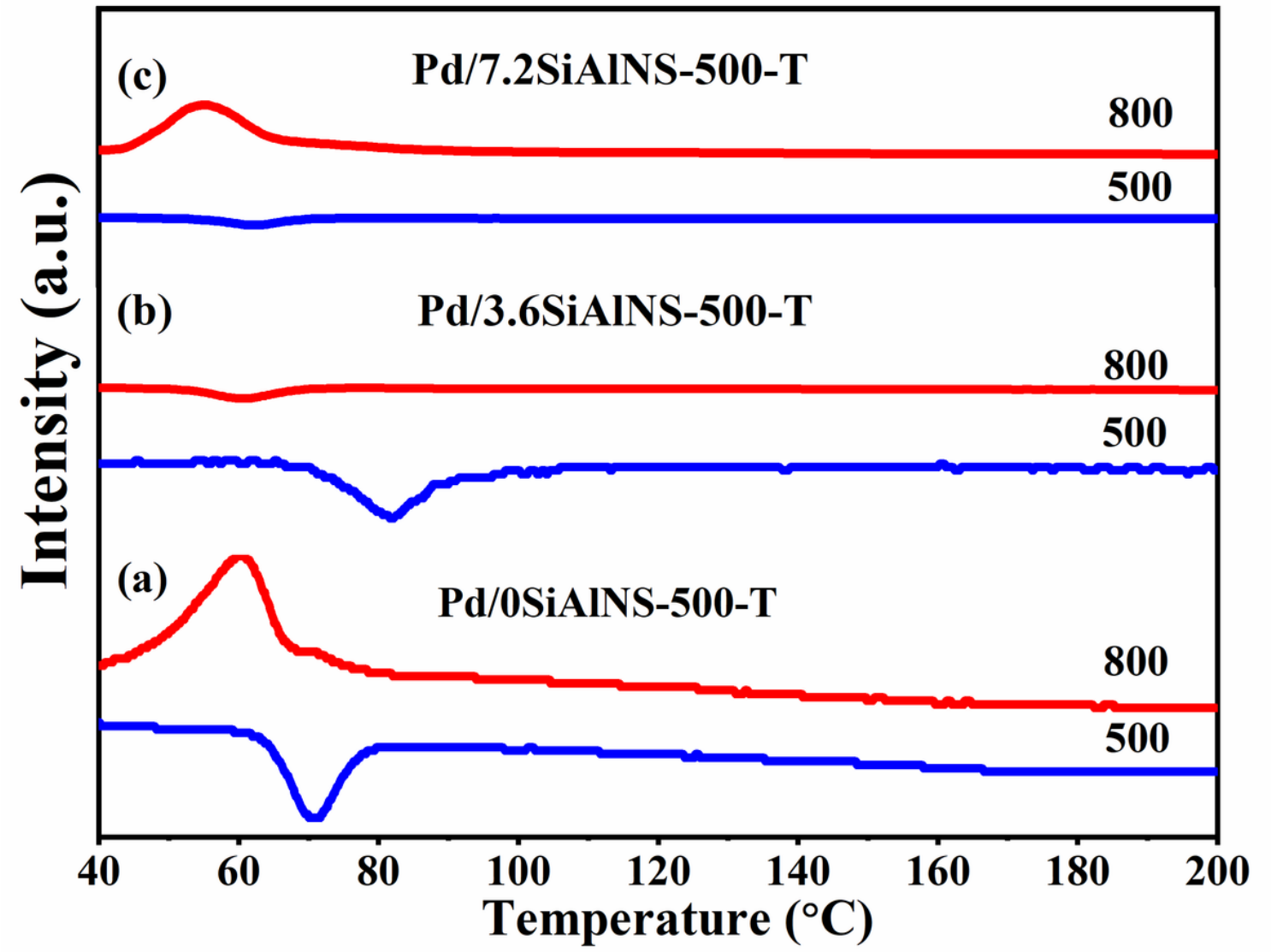

Figure 5

H2-TPR patterns of Pd/0SiAlNS-500-T (a), Pd/3.6SiAlNS-500-T (b) and Pd/7.2SiAlNS-500-T (c) catalysts calcined at 500 °C and 800 ℃

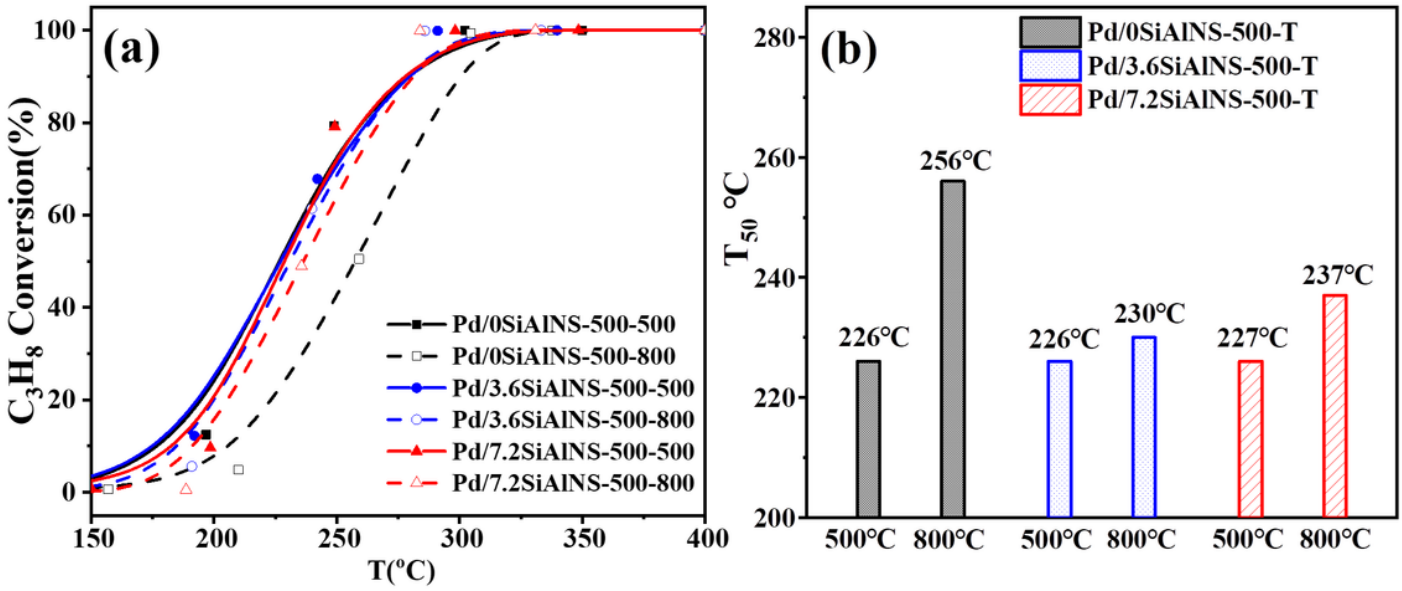

Figure 6

Light-off curves (a) and T50 (b) of fresh and aged Pd/XSiAlNS-500 catalysts at 800 ℃ for catalytic combustion of propane

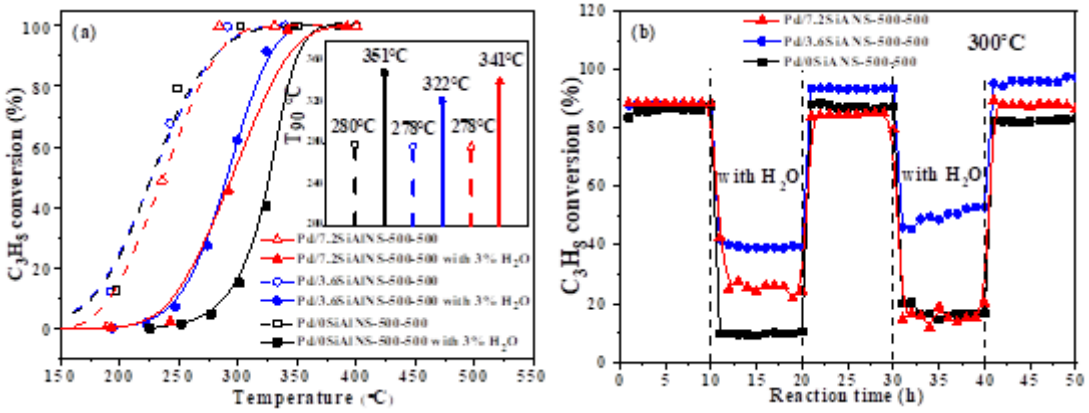

Figure 7

Light-off curves (a) and stability at 300 ℃ (b) of Pd/XSiAlNS-500-500 catalysts for catalytic combustion of propane under the humid conditions (3% H2O)